

# Dynamic holography in a broad-area optically pumped vertical GaAs microcavity

David D. Nolte and Karrin M. Kwolek

*Department of Physics, Purdue University, West Lafayette, Indiana 47907-1396*

Chet Lenox and Ben Streetman

*University of Texas, Austin, Texas 78712*

Received January 1, 2000; revised manuscript received November 6, 2000

A broad-surface-area vertical GaAs microcavity was operated as an adaptive holographic film. The cavity mirrors were transparent to high-energy (millijoules per square centimeter) hologram writing pulses at a wavelength of 730 nm that generated optically pumped gain gratings in a 1- $\mu\text{m}$ -thick active layer of GaAs. The gain gratings were probed with a low-intensity (mW) tunable laser at wavelengths near the GaAs band edge in the high-reflectance bandwidth of the cavity Bragg mirrors. When the structure was designed with low mirror reflectances [ $(R_1R_2)^{1/2} = 90\%$ ] to operate below the lasing threshold, the cavity resonance bandwidth was sufficiently broad to permit homogeneous hologram readout over a large (several square millimeters) area. Diffraction efficiencies of approximately 10% were predicted and approached experimentally. These results represent a first step toward the realization of a holographic vertical-cavity surface-emitting laser structure. © 2001 Optical Society of America

OCIS codes: 090.2900, 140.5960, 190.5970, 230.1150, 160.3380, 050.1970.

## 1. INTRODUCTION

Adaptive optics encompasses both active and passive feedback systems that respond to changing optical conditions. Active adaptive systems require a detailed model of system response coupled with sensitive detection and actuators, whereas passive adaptive systems have the advantage that no active monitoring or control is necessary. Adaptive holographic films have several advantages as passive adaptive systems; for instance, diffraction from thin films generates multiple diffraction orders in the Raman–Nath regime, alleviating the need for critical Bragg-angle matching during readout. In addition, access to the multiple diffraction orders, each containing a different combination of the conjugated amplitudes of the write and probe beams, can be separate and simultaneous. One can use different combinations in the different orders to perform multiple functions, such as correlation, phase conjugation, and convolution.

The most sensitive dynamic holographic media are semiconductor heterostructures operated at wavelengths near the fundamental bandgap.<sup>1</sup> Photorefractive quantum wells<sup>2,3</sup> (PRQW's) are simple and versatile examples of semiconductor adaptive holographic film. These devices have the highest holographic writing sensitivity of any material system studied to date, with  $S_2 = 1 \times 10^7 \text{ cm}^2/\text{W}$ .<sup>3</sup> They have relatively high dynamic hologram writing and erase speeds that approach 1 MHz.<sup>4</sup> They can be operated in multiple configurations, including simple configurations that are easy to fabricate and have excellent longevity in operation.<sup>5</sup> Applications of PRQW devices include image processing,<sup>6,7</sup> adaptive laser-based ultrasound detection,<sup>8,9</sup> optically programmable femtosecond pulse shaping,<sup>10–12</sup> and imaging

through turbid media.<sup>13,14</sup> Each of these applications uses the high sensitivity and high speed of the PRQW devices in addition to their adaptability to changing optical conditions in which they compensate for vibrations, speckle, and scattered light.

The diffraction efficiency of photorefractive quantum wells is fundamentally limited to only several percent, even when one is using microcavity enhancements,<sup>15</sup> because the PRQW's rely intrinsically on an absorptive optical nonlinearity. This has limited their use to single-stage applications. It has not yet been possible to cascade the PRQW devices. In addition to cascaded applications, there are applications for which even the megahertz response rate of the PRQW is too slow. Although dynamic compensation for dispersion in femtosecond pulses has been demonstrated,<sup>16</sup> it has not been possible to operate at sufficient speeds to compensate for dispersion in changing data packets, which would allow this application to be useful for telecommunications. Therefore there is a clear need to extend the development of adaptive holographic films to higher diffraction efficiencies and higher speeds.

One way in which to extend adaptive holographic films is to remove the optical absorption, replacing it with optical gain. This approach has been successfully pursued in dynamic holography in active laser media. Holographic lasers, four-wave mixing, and phase conjugation in laser crystals and holographic oscillators have been demonstrated in YAG, vanadate, and Ti:sapphire crystals that use gain gratings as holographic elements.<sup>17–22</sup> Semiconductors can also have optical gain when they are optically or electrically pumped. Typical laser gain in GaAs is near  $g = 300 \text{ cm}^{-1}$ . This value is sufficient for semi-

conductor waveguide lasers that have interaction lengths of the order of 1 mm. However, for a thin film that is only 1  $\mu\text{m}$  thick, the single-pass gain is only  $gL = 3\%$ . Therefore, to utilize the intrinsic amplification associated with the weak gain in a semiconductor thin film, it is necessary to incorporate the film into a vertical cavity with high mirror reflectances. Such a structure for the gain-grating adaptive holographic film is similar to a vertical-cavity surface-emitting laser (VCSEL) structure.

Surface-emitting lasers have been studied extensively in response to the need for micrometer-sized light emitters for integration with microelectronic systems. Because of their small size and suitability for use in large arrays, VCSEL's in particular have a distinct advantage over edge-emitting semiconductor diode lasers.<sup>23</sup> A typical VCSEL has an active region consisting of a few quantum wells sandwiched between two reflectors. Mirror tolerances in VCSEL's are very stringent, with reflectivity  $R > 99\%$ . Such high-finesse cavities have narrow cavity resonances, of the order of  $<0.01\%$  of the optical frequency, whereas the gain region bandwidth is considerably larger.<sup>24</sup> Molecular-beam epitaxy growth tolerances of 1% are required for overlap between the cavity resonance and gain regions.<sup>24</sup>

Our long-term goal is to use VCSEL structures as adaptive holographic films without reticulation of the VCSEL into laser arrays. The device would be accessible to optically written gain-grating holograms that can be read out with greater-than-unity diffraction efficiency. As a first step toward this goal, we fabricated an optically pumped (nonlasing) vertical-cavity structure in which we tested the feasibility of matching molecular-beam-epitaxy growth of cavity structures with the requirements of broad-area (several square millimeters) homogeneity for holographic applications. The condition of homogeneity in cavity resonance (set by the thickness of the cavity) made it necessary to work initially with low cavity-mirror reflectances that permitted relatively broadband (several nanometers) operation. The high mirror losses do not permit net gain in the structure, but all other aspects of the role of generating and probing gain gratings in the structure could be explored.

We present the details of the cavity structure in Section 2, with an explanation of our choice of cavity reflectances and thicknesses that make this structure considerably different from conventional VCSEL structures. The predicted performance of optical grating writing in the structure and dynamic diffraction from the gain gratings, including wavelength and intensity dependences, is presented in Section 3. The experimental studies, which semiquantitatively match the predicted performance, are described in Section 4. In the final section we discuss future directions for research and describe what the current research tells us as we move toward an eventual holographic VCSEL structure.

## 2. HOLOGRAPHIC GaAs MICROCAVITY

For holographic applications of thin films a primary operating parameter is the readable bandwidth of the hologram, i.e., the wavelength range of the readout laser for which the hologram's diffraction efficiency is relatively

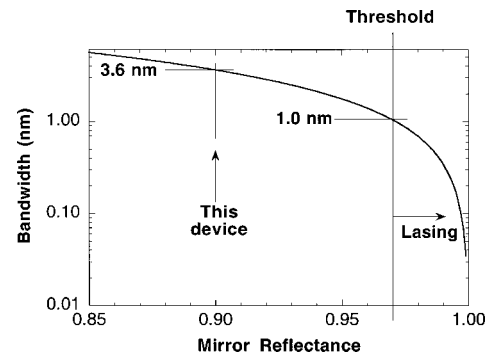


Fig. 1. Calculated cavity bandwidth versus joint mirror reflectance  $(R_1R_2)^{1/2}$ . The gain threshold at 97% is calculated for a 1- $\mu\text{m}$  GaAs active layer that has saturated gain. The bandwidth of the microcavity structure grown at UT Austin is approximately 3.6 nm.

constant. For nearly all applications, this bandwidth should be as large as possible to alleviate laser-tuning requirements as well as to accommodate design and fabrication processes of the holographic film that may produce spatially varying shifts in the center operating wavelength. Useful holographic films must operate as wide-area devices (square millimeters and greater), and the strength of the hologram should be uniform across this area. If the hologram readout bandwidth is too small, these spatially dependent shifts will prevent uniform readout. Therefore designing a useful holographic microcavity requires relatively broadband operation.

The broadband requirement for holographic films is incompatible with the performance of conventional microcavity lasers. Laser-cavity mirror reflectances are set high to limit losses. The bandwidth of a cavity with one high-reflector mirror and an output coupler with reflectance  $R$  is given by

$$\text{BW} = \frac{\nu_F}{F} = \frac{C(1-R)}{2L\pi\sqrt{R}}, \quad (1)$$

where  $\nu_F$  is the free spectral range,  $F$  is the finesse, and  $L$  is the thickness of the cavity. The cavity bandwidth for a GaAs microcavity is shown in Fig. 1 as a function of the output coupler's reflectance (assuming that the bottom mirror is a high reflector). For instance, reflectances greater than 99% produce cavity bandwidths that are a small fraction of a nanometer. To achieve a bandwidth of 3.6 nm requires an output coupler reflectance as low as 90%.

Such a low reflectance for the cavity subsequently requires that the thickness of the cavity nonlinear medium (GaAs) be as large as possible to provide sufficient interaction length to produce large diffraction efficiency. Although the bandwidth decreases inversely with cavity length, the diffraction efficiency grows as the square of the interaction length. Therefore the need for broadband holographic films with high diffraction efficiency requires a compromise between cavity thickness and cavity reflectance. Optimizing the structures causes holographic microcavities to be much thicker than are typically found in conventional microcavities or VCSEL's, which have thicknesses that are usually only fractions of a micrometer.<sup>25</sup> The gain threshold is determined by

$$\text{gain}_{\text{th}} = \frac{1}{2L} \ln R. \quad (2)$$

The gain threshold for an active layer of 1  $\mu\text{m}$  of GaAs on a high reflector occurs at an output coupler reflectance of 97%, shown as the threshold in Fig. 1.

The structure of the holographic microcavity that we designed and grew is shown in Fig. 2. The structure consists of a 1- $\mu\text{m}$ -thick GaAs active layer sandwiched between a bottom Bragg stack of 10 periods of 61.6 nm  $\text{Al}_{0.1}\text{Ga}_{0.9}\text{As}/72.8\text{ nm AlAs}$  and a top Bragg stack consisting of 5 periods of 61.6 nm  $\text{Al}_{0.1}\text{Ga}_{0.9}\text{As}/72.8\text{ nm AlAs}$ . The center wavelengths of the Bragg stacks are centered at 870 nm. The bottom and top Bragg mirrors have reflectances of 97% and 93% respectively, with a reflectance product of 90%. Therefore this structure is not a laser structure (shown in Fig. 1) because the output coupler produces higher loss than can be balanced by laser gain in the 1- $\mu\text{m}$  GaAs layer.

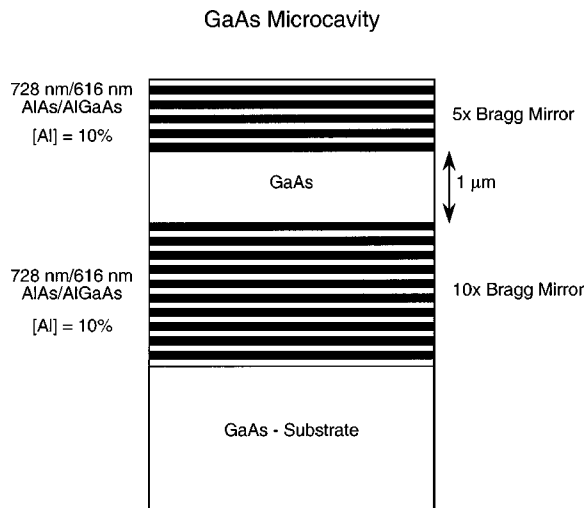


Fig. 2. Vertical GaAs microcavity structure grown at UT Austin. The 1- $\mu\text{m}$  active-layer thickness provides a long interaction length to compensate partially for the low mirror reflectances that were chosen to yield the wide bandwidth that is necessary for broad-area holography.

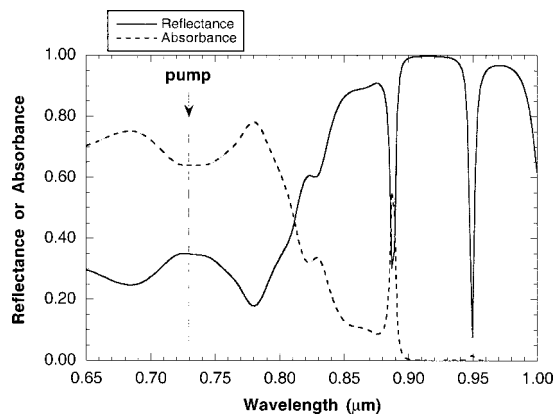


Fig. 3. Calculated reflectance and absorbance spectra of the UT Austin microcavity. The probe and pump wavelengths used in the experiments are indicated. The top mirror is transparent to the pump light at 730 nm but reflective at the probe wavelength near 870 nm.

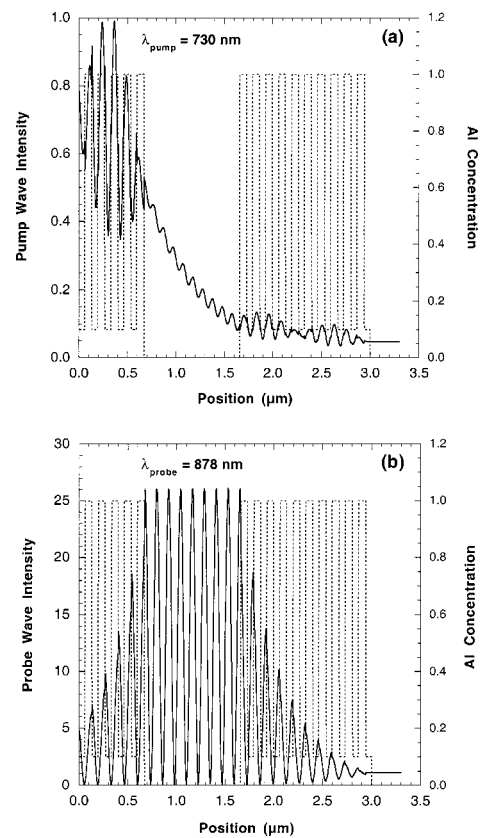


Fig. 4. Calculated intensities inside the structure for the pump and probe waves. Note the difference in vertical scale between the two figures. The structure rests upon a GaAs substrate.

The calculated external reflectance for the structure in Fig. 2 is shown in Fig. 3 for a cavity thickness chosen to place the cavity resonance at the edge of the GaAs absorption. The thick cavity produces a small free spectral range  $\nu_F$ , which produces additional cavity resonances at nearby wavelengths. (The small free spectral range has a practical benefit in the experiments by ensuring that the usual thickness variations across the wafer induced by the molecular-beam epitaxy growth process will bring a cavity resonance into coincidence with the GaAs band edge at some locations on the wafer.) The bandwidths of the Bragg mirrors are clearly discernible in the figure and span the range 800–1000 nm.

In our experiment, described below, we optically pumped gain gratings, using a pump wavelength of 730 nm, while probing the holographic gain gratings with a wavelength tuned to the cavity resonance at the band edge of GaAs at 870 nm. An important aspect of this microcavity design is the relative transparency of the top reflector to the optical pump at a wavelength of 730 nm. This mirror allows the pump light to penetrate the mirrors and to be absorbed by the GaAs layer inside the cavity while providing high reflectance for the resonant wavelength near 870 nm. The absorbance of the structure is shown in Fig. 3, from which we can observe the relatively high absorption at the pump wavelength. The calculated intensity of the pump wave inside the cavity is shown in Fig. 4. The intensity of the probe wavelength is also shown. Note the difference in scales between the pump and probe. The pump was absorbed predomi-

nantly in the GaAs layer, although a small fraction of the pump energy was absorbed in the output coupler mirror. A small amount of energy leaked through the high reflector to the GaAs substrate.

### 3. CALCULATED HOLOGRAPHIC PERFORMANCE

The linear, nonlinear, and holographic optical properties of the holographic microcavity were calculated by the theoretical transfer matrix approach of Ref. 15. The value of the absorption of GaAs under high excitation was taken from Ref. 1, and the refractive index was calculated from a Kramers–Kronig transformation of the absorption data. These material properties were fixed, and the optical properties were calculated for the specific structure that was grown and studied here. Although the modeling contains many parameters, most were determined by the specific structure under study. The principal adjustable parameter in the calculations was the thickness of the GaAs layer of the cavity.

The calculated reflectance of the microcavity is shown in Fig. 5 for dark and pumped conditions, assuming an optically pumped carrier density of  $1 \times 10^{18} \text{ cm}^{-3}$ . This carrier density produces gain in the GaAs, but the low mirror reflectivity prevents operation of the microcavity as a laser. The principal effect of the optical pumping is mode pulling of the cavity resonance, which produces strong spatial modulation of the reflectance at wavelengths near the resonance. Spatial modulation of the pump intensity, through the interference of the holographic writing process, therefore produces a strong reflectance grating that diffracts the probe beam.

The calculated dark reflectance spectra of the microcavity, for several cavity thicknesses spanning a 100-nm range, are shown in Fig. 6(a). The associated predicted diffraction efficiencies are shown in Fig. 6(b). The resonant enhancement in the diffraction efficiency near the GaAs band edge is plainly visible, with a peak predicted diffraction efficiency of approximately 10% for an optically pumped carrier density of  $1 \times 10^{18} \text{ cm}^{-3}$ . The diffraction efficiency is shown in Fig. 7 as a function of carrier density. Diffraction efficiencies for this structure

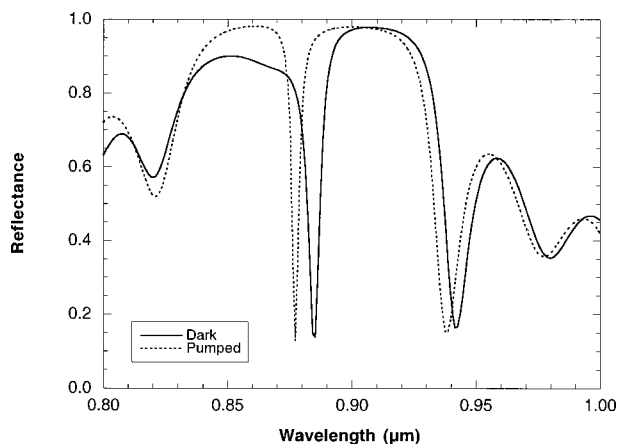


Fig. 5. Calculated reflectance for the structure in the dark and pumped with a carrier density of  $1 \times 10^{18} \text{ cm}^{-3}$ , showing the mode pulling of the cavity resonance.

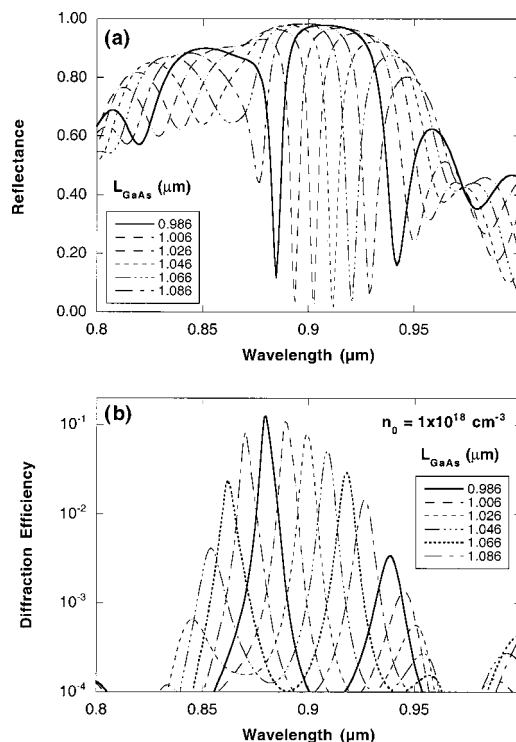


Fig. 6. (a) Calculated reflectance and (b) diffraction efficiency versus cavity thickness. Diffraction efficiencies of 10% are predicted for the structure under an excited carrier concentration of  $1 \times 10^{18} \text{ cm}^{-3}$  when the cavity resonance is slightly below the energy of the GaAs band edge.

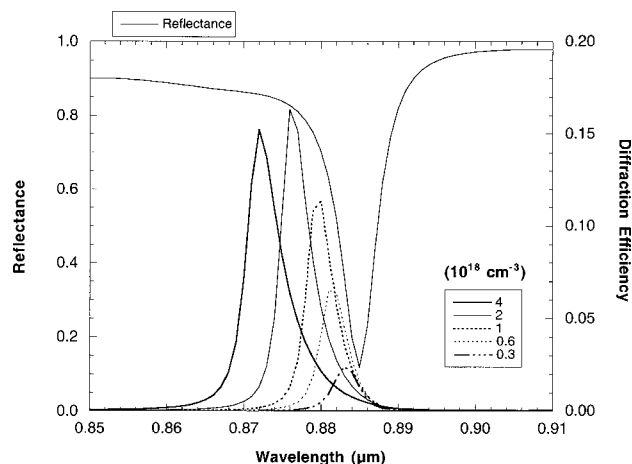


Fig. 7. Calculated diffraction efficiency versus carrier density, showing the mode pulling and saturation at high excitation. The dark reflectance is also shown.

should approach 15% for a density of  $2 \times 10^{18} \text{ cm}^{-3}$ . The calculations predict a nonlinear increase in the diffraction peak with increasing pump fluence as well as mode pulling of the peak to higher energies. Saturation of the gain gratings is reflected in saturation of the diffraction efficiency for higher carrier densities.

### 4. EXPERIMENTAL STUDIES

The holographic microcavity was grown by Chet Lenox at the University of Texas at Austin (UT Austin) in collabo-

ration with Streetman, one of the present authors. Unlike for a photorefractive asymmetric Fabry–Perot interferometer<sup>26</sup> or a VCSEL,<sup>24</sup> no postgrowth processing or fabrication of the holographic microcavity is required. Figure 8 shows selected reflectances from the device surface of an ~1.0-mm-diameter cw probe beam centered at 10 positions located 1.5 mm apart on a 9 × 3 grid.

Nondegenerate four-wave mixing experiments were performed with a XeCl excimer-pumped Pyridine 2 pulsed dye laser, yielding 20-ns pulses at 730 nm to write the carrier gratings with a fringe spacing of 40 μm. A cw Ti:sapphire laser was then used to probe the gratings. The experimental configuration is shown in Fig. 9. The first-order diffracted signal was detected with a 125-MHz (8-ns) bandwidth amplified silicon photodiode. The signal was averaged on a 500-MHz (2-ns) storage oscilloscope. Deconvolution of the detected signal with the system response yielded approximately a factor of 2.

The dark reflectance and the diffraction efficiency for an optical pump intensity of 1 mJ/cm<sup>2</sup> are shown in Fig. 10 for a set of cavity thicknesses measured at several positions across the VCSEL wafer. The diffraction efficiency shows a pronounced maximum near the semiconductor bandgap when the cavity resonance occurs at the band edge. The measured diffraction efficiency falls off as the resonant wavelength of the cavity shifts higher or lower than the band-edge wavelength. The qualitative behavior of the data is correctly modeled by the results in Fig. 6, but the quantitative aspects differ in some detail. The most pronounced differences are that the depths of the measured reflectance resonances were smaller than predicted; the measured diffraction efficiencies were smaller than predicted, even after deconvolution with the

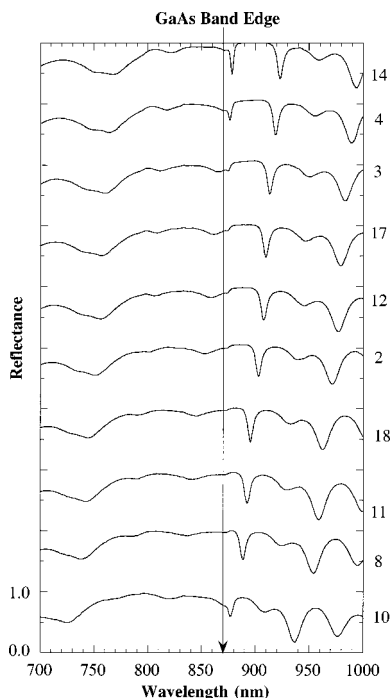


Fig. 8. Measured reflectance versus thickness for the UT Austin structure at several locations across the wafer. Varying the location on the wafer allows the resonance to be tuned into the band edge of the GaAs active layer.

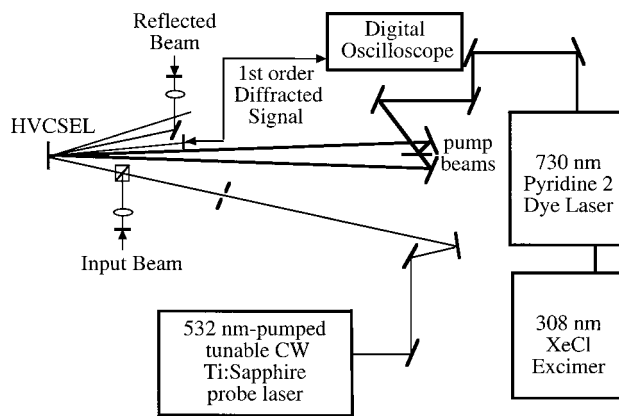


Fig. 9. Experimental setup for generating optically pumped gain gratings probed by a tunable cw Ti:sapphire laser. The pump fluence can be varied up to several millijoules per square centimeter. HVCSEL, holographic vertical-cavity surface-emitting laser.

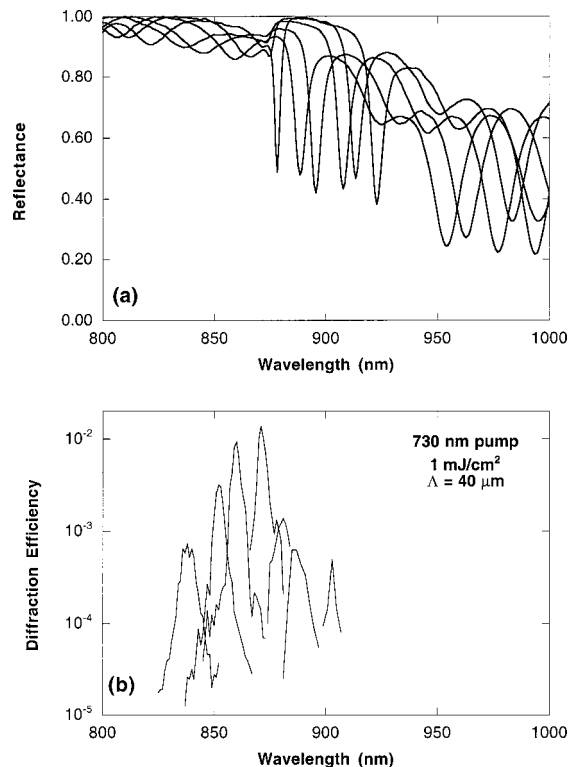


Fig. 10. (a) Measured reflectance and (b) diffraction efficiency for several cavity conditions across the wafer. The diffraction efficiencies have not been corrected for the system response. The data show semiquantitative agreement with the behavior calculated in Fig. 6. Differences between the calculated and the measured responses are described and explained in the text.

system response; and the measured peak diffraction efficiency decreased more rapidly than predicted as the resonance was tuned below the bandgap.

There are several possible sources of the quantitative discrepancy between prediction and experiment. Most importantly, the thickness variation of the growth produces a distribution of narrow cavity resonances over a sampling region of several square millimeters for both the reflectance measurements and the diffraction measure-

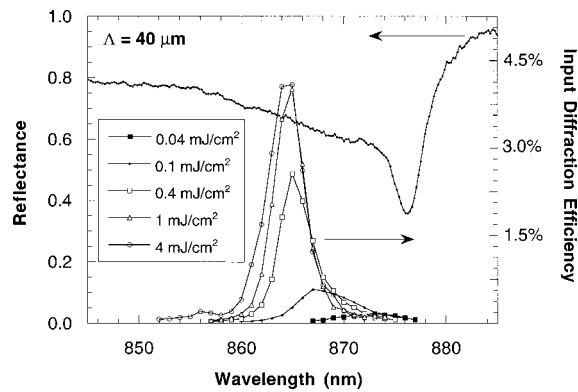


Fig. 11. Measured diffraction efficiency (not corrected for system response) versus pump fluence, showing mode pulling and saturation, in semiquantitative agreement with the behavior calculated in Fig. 7.

ments. This distribution of resonance wavelengths broadens the experimentally measured spectral lines, with a concomitant decrease in the peak values. The falloff of the peak diffraction signal when the cavity resonance shifts below the bandgap may be due to systematics in the data analysis and to the method used to extract the free-carrier nonlinearities from the influence of thermal gratings.

The fluence dependence of the diffraction is shown in Fig. 11 along with the reflectance at a single spot on the holographic microcavity. The data agree reasonably well with the calculations of Fig. 7, showing a marked increase in the diffraction for intensities up to  $1 \text{ mJ/cm}^2$  followed by saturation of the diffraction at higher intensities. The peak in the diffraction also shows the same mode pulling as in the calculations, shifting to higher energy with increasing excitation. The saturation of the mode pulling in the data is not seen in the calculations but may be due to thermal heating of the lattice in the experiment, which would produce a wavelength shift that would compete with the mode pulling.

## 5. CONCLUSIONS

In conclusion, we have operated a GaAs microcavity as a holographic thin film, using optically pumped gain gratings over a broad area (square millimeters). Diffraction efficiencies near 10% were calculated and approached in the nonlasing structure. This study has allowed us to validate our numerical model as well as to validate the ability to perform dynamic holography in microcavities that closely resemble VCSEL structures. The next step will be the design and testing of a holographic VCSEL. Our numerical model predicts diffraction efficiencies approaching 100% in these structures.

## ACKNOWLEDGMENT

The authors acknowledge support from National Science Foundation grant ECS-9708230.

D. D. Nolte's e-mail address is nolte@physics.purdue.edu.

## REFERENCES

- H. Haug and S. W. Koch, *Quantum Theory of the Optical and Electronic Properties of Semiconductors* (World Scientific, Singapore, 1990).
- D. D. Nolte and M. R. Melloch, "Photorefractive quantum wells and thin films," in *Photorefractive Effects and Materials*, D. D. Nolte, ed. (Kluwer Academic, Dordrecht, The Netherlands, 1995), pp. 373–451.
- D. D. Nolte, "Semi-insulating semiconductor heterostructures: Optoelectronic properties and applications," *J. Appl. Phys.* **85**, 6259–6289 (1999).
- S. Balasubramanian, I. Lahiri, Y. Ding, M. R. Melloch, and D. D. Nolte, "Two-wave mixing dynamics and nonlinear hot-electron transport in transverse-geometry photorefractive quantum wells studied by moving gratings," *Appl. Phys. B* **68**, 863–869 (1999).
- Q. N. Wang, R. M. Brubaker, D. D. Nolte, and M. R. Melloch, "Photorefractive quantum wells: transverse Franz-Keldysh geometry," *J. Opt. Soc. Am. B* **9**, 1626–1641 (1992).
- A. Partovi, A. M. Glass, T. H. Chiu, and D. T. H. Liu, "High-speed joint-transform optical image correlator using GaAs/AlGaAs semi-insulating multiple quantum wells and laser diodes," *Opt. Lett.* **18**, 906–908 (1993).
- W. S. Rabinovich, S. R. Bowman, R. Mahon, A. Walsh, G. Beadie, L. Adler, D. S. Katzer, and K. Ikossi Anastasiou, "Gray-scale response of multiple quantum well spatial light modulators," *J. Opt. Soc. Am. B* **13**, 2235–2241 (1996).
- I. Lahiri, D. D. Nolte, M. R. Melloch, and M. B. Klein, "Oscillatory mode coupling and electrically strobed gratings in photorefractive quantum-well diodes," *Opt. Lett.* **23**, 49–51 (1998).
- I. Lahiri, L. J. Pyrak-Nolte, D. D. Nolte, M. R. Melloch, R. A. Kruger, G. D. Bacher, and M. B. Klein, "Laser-based ultrasound detection using photorefractive quantum wells," *Appl. Phys. Lett.* **73**, 1041–1043 (1998).
- Y. Ding, D. D. Nolte, M. R. Melloch, and A. M. Weiner, "Time-domain image processing using dynamic holography," *IEEE J. Sel. Top. Quantum Electron.* **4**, 332–341 (1998).
- Y. Ding, R. M. Brubaker, D. D. Nolte, M. R. Melloch, and A. M. Weiner, "Femtosecond pulse shaping by dynamic holograms in photorefractive multiple quantum wells," *Opt. Lett.* **22**, 718–721 (1997).
- Y. Ding, D. D. Nolte, M. R. Melloch, and A. M. Weiner, "Real-time edge enhancement of femtosecond time-domain images by use of photorefractive quantum wells," *Opt. Lett.* **22**, 1101–1103 (1997).
- R. Jones, M. Tziraki, P. M. W. French, K. M. Kwolek, D. D. Nolte, and M. R. Melloch, "Direct-to-video holographic 3-D imaging using photorefractive multiple quantum well devices," *Opt. Express* **2**, 439–448 (1998); <http://epubs.osa.org/opticsexpress>.
- R. Jones, N. P. Barry, S. C. W. Hyde, P. M. W. French, K. M. Kwolek, D. D. Nolte, and M. R. Melloch, "Direct-to-video holographic readout in quantum wells for 3-D imaging through turbid media," *Opt. Lett.* **23**, 103–105 (1998).
- D. D. Nolte and K. M. Kwolek, "Diffraction from a short-cavity Fabry-Perot: applications to photorefractive quantum wells," *Opt. Commun.* **115**, 606–616 (1995).
- Y. Ding, A. M. Weiner, M. R. Melloch, and D. D. Nolte, "Adaptive all-order dispersion compensation of ultrafast laser pulses using dynamic spectral holography," *Appl. Phys. Lett.* **75**, 3255–3257 (1999).
- M. J. Damzen, R. P. M. Green, and K. S. Syed, "Self-adaptive solid-state laser oscillator formed by dynamic gain-grating holograms," *Opt. Lett.* **20**, 1704–1706 (1995).
- A. Brignon and J. P. Huignard, "Energy efficiency of phase conjugation by saturable-gain degenerate four-wave mixing in Nd: YAG amplifiers," *Opt. Commun.* **119**, 171–177 (1995).
- M. J. Damzen, S. Camacho Lopez, and R. P. M. Green, "Wave-mixing and vector phase conjugation by polarization-dependent saturable absorption in  $\text{Cr}^{4+}:\text{YAG}$ ," *Phys. Rev. Lett.* **76**, 2894–2897 (1996).

20. K. S. Syed, G. J. Crofts, R. P. M. Green, and M. J. Damzen, "Vectorial phase conjugation via four-wave mixing in isotropic saturable-gain media," *J. Opt. Soc. Am. B* **14**, 2067–2078 (1997).
21. R. P. M. Green, D. Udaiyan, G. J. Crofts, D. H. Kim, and M. J. Damzen, "Holographic laser oscillator which adaptively corrects for polarization and phase distortions," *Phys. Rev. Lett.* **77**, 3533–3536 (1996).
22. A. Brignon, L. Loiseau, C. Larat, J. Huignard, and J. Pocholle, "Phase conjugation in a continuous-wave diode-pumped Nd:YVO<sub>4</sub> laser," *Appl. Phys. B* **69**, 159–162 (1999).
23. H. C. Casey and M. B. Panish, *Heterostructure Lasers* (Academic, New York, 1978).
24. J. L. Jewell, J. P. Harbison, A. Scherer, Y. H. Lee, and L. T. Florez, "Vertical-cavity surface-emitting lasers: design, growth, fabrication, characterization," *IEEE J. Quantum Electron.* **27**, 1332–1346 (1991).
25. T. E. Sale, *Vertical Cavity Surface Emitting Lasers* (Wiley, New York, 1995).
26. K. M. Kwolek, M. R. Melloch, D. D. Nolte, and G. A. Brost, "Diffractive quantum-well asymmetric Fabry–Perot: transverse-field photorefractive geometry," *Appl. Phys. Lett.* **67**, 736–738 (1995).